


## Sequential deprotonation of the allene trication produced by 30-keV/u He<sup>2+</sup> impact

Zhencen He<sup>✉,1</sup>, Jiarong Wang<sup>✉,1</sup>, Yu Zhang<sup>2,\*</sup>, Bo Wang<sup>1</sup>, Jie Han<sup>1</sup>, Baihui Ren<sup>1</sup>, Long Wei<sup>✉,1</sup>, Zihan Xia<sup>1</sup>, Pufang Ma<sup>1</sup>, Tianming Meng<sup>1</sup>, Yaming Zou<sup>1</sup>, Zhimin Hu<sup>3,†</sup> and Baoren Wei<sup>✉,1,‡</sup>

<sup>1</sup>*Institute of Modern Physics, Key Laboratory of Nuclear Physics and Ion-Beam Application (MOE), Fudan University, Shanghai 200433, China*

<sup>2</sup>*College of Data Science, Jiaying University, Jiaying 314001, China*

<sup>3</sup>*Key Laboratory of Radiation Physics and Technology of Ministry of Education, Institute of Nuclear Science and Technology, Sichuan University, Chengdu 610064, China*

 (Received 22 November 2021; revised 26 January 2022; accepted 10 February 2022; published 22 February 2022)

The three-body fragmentation channel  $H^+ + H^+ + C_3H_2^+$  of the allene trication produced by 30-keV/u He<sup>2+</sup> ion impact is investigated using cold-target recoil-ion momentum spectroscopy. The two protons with different kinetic energies are found emitted sequentially from the parent trication. The presence of such a sequential deprotonation process and the absence of corresponding concerted deprotonation may result from a major molecular deformation process, e.g., ultrafast hydrogen migration, which occurs in the parent ion prior to fragmentation, and finally leads to the formation of two different protons.

DOI: [10.1103/PhysRevA.105.022818](https://doi.org/10.1103/PhysRevA.105.022818)

### I. INTRODUCTION

The three-body fragmentation of multicharged polyatomic molecules has drawn much attention recently, since it can serve as a diagnostic tool to probe the structural and dynamical information during molecular dissociation, e.g., molecular geometry reconstructed by Coulomb explosion imaging [1–3], lifetime of metastable intermediate ions [4–8], and direct observation of roaming processes [9]. The precursor molecular cations can decay into three fragments via concerted or sequential pathways, which depend on whether a metastable intermediate ion could be formed or not. If the intermediate ion cannot survive for a time larger or comparable to the molecule vibrational and rotational period, concerted fragmentation would be preferred [10–12]. Otherwise such two kinds of pathways could coexist [13–15] and their ratios can be controlled by the parameters of ionizing particles [15–18]. However, for some larger molecules the sequential mechanism becomes dominant [19], as the relatively small Coulomb repulsion forces among the corresponding parts within the molecules could not break the molecular bonds concertedly.

Allene (CH<sub>2</sub>CCH<sub>2</sub>), as one isomer of C<sub>3</sub>H<sub>4</sub>, possesses a linear carbon skeleton. Its ionization and dissociation processes have been investigated to obtain information concerning the isomer effect [20,21], fragmentation patterns [20–26], and intramolecular hydrogen migration [23,24]. The three-body fragmentation dynamics of allene trication has been measured under 50-keV/u Ne<sup>8+</sup> collisions [22] and strong laser field ionization [23,24], but only two channels, i.e.,  $H^+ + CH^+ + C_2H_2^+$  and  $H^+ + CH_2^+ + C_2H^+$ , were

concerned. Another important channel  $H^+ + H^+ + C_3H_2^+$  was not reported. Similar channels involving the production of two protons have been observed in the dissociation of C<sub>2</sub>H<sub>2</sub> [15,16] and C<sub>2</sub>H<sub>4</sub> [17,18] trications. In these cases, the two protons can be emitted concertedly or sequentially. However, less is known on the two-proton emission pattern in the allene trication fragmentation and on the role of hydrogen-migration-induced isomerization for the  $H^+ + H^+ + C_3H_2^+$  channel. The isomerization via 1,2-H migration has been theoretically predicted to play an essential role in the dissociation of allene cations [27]. Such an isomerization process is faster than dissociation since the isomerization barrier is rather lower than the dissociation barrier. The hydrogen-migration-induced isomerization has been experimentally observed in the dissociation of C<sub>3</sub>H<sub>4</sub> dications [25], as well as trications forming  $H^+ + CH^+ + C_2H_2^+$  and  $H^+ + CH_2^+ + C_2H^+$  [23,24]. The timescale of hydrogen migration involved in the trication channels has been estimated to be ~20 fs [24]. In the following, the C<sub>3</sub>H<sub>4</sub> molecule is referred to as an allene unless otherwise stated.

To better understand the three-body molecular fragmentation dynamics, in the present paper we pay particular attention to the three-body channel  $H^+ + H^+ + C_3H_2^+$  of C<sub>3</sub>H<sub>4</sub><sup>3+</sup> trications induced by 30-keV/u He<sup>2+</sup> impact. Utilizing the cold-target recoil-ion momentum spectroscopy (COLTRIMS) technique [28], the complete kinematics of channels of interest are measured, thus allowing the identification of the fragmentation mechanism with the aid of the Dalitz plot and Newton diagram analysis.

### II. EXPERIMENTS AND DATA ANALYSIS

The present experiment was carried out using a COLTRIMS setup mounted on the 150-kV highly charged ion collision platform at Fudan University. Details can be found

\*zyclay@outlook.com

†huzhimin@scu.edu.cn

‡brwei@fudan.edu.cn

in our previous work [15,29], so here only a brief description will be given. A 30-keV/u He<sup>2+</sup> ion beam perpendicularly crossed a cold supersonic jet produced by pure allene gas with a pressure of 1 bar passing through a 20- $\mu$ m nozzle into a high vacuum collision chamber. After an interaction, the recoil ions were produced due to the ionization and dissociation of molecules. These ions were extracted from the interaction zone to fly through the acceleration section and field-free section, and finally detected by a position-sensitive detector (PSD) equipped with two multichannel plates and a delay-line anode. The uniform extraction field along the time-of-flight (TOF) spectrometer axis was 60 V/cm, which ensured recoil ions with a kinetic energy up to  $\sim 5.5$  eV could be completely collected. Simultaneously, the scattered projectiles were charge separated by an electrostatic deflector and detected by another PSD. In the coincidence measurement, the TOF of the recoil ions was determined by taking the scattered projectile signal as a reference, and recorded by a multihit time-to-digital converter. The three-dimensional momenta of all recoil ions were reconstructed from the hitting TOF and position information.

According to the dependence of TOF on the mass-to-charge ratio, ion species were identified. The fragmentation channels were distinguished from the coincidence TOF map. In order to identify the fragmentation mechanism in a three-body fragmentation process, the Dalitz plot and Newton diagram were utilized to reveal the momentum correlations [4]. In a Dalitz plot, data points are plotted within a circle inscribed in an equilateral triangle. The coordinates  $X$  and  $Y$  corresponding to each data point are given by

$$X = \frac{p_1^2 - p_2^2}{\sqrt{3} \sum p_i^2}, \quad (1)$$

$$Y = \frac{p_3^2}{\sum p_i^2} - \frac{1}{3}, \quad (2)$$

where  $p_i$  with  $i = 1, 2, 3$  represent the momenta of the first, second, and third detected ions, respectively. In a Newton diagram, the momentum vector of the first fragmentation ion is represented by an arrow along the horizontal axis fixed to one arbitrary unit. The momentum vectors of the second and third fragments are normalized using the same normalization factor for the first fragment and placed in the upper and lower halves of the plot, respectively.

To confirm the sequential fragmentation mechanism, the Dalitz plot can be Monte Carlo simulated using a classical mechanical model. In a pure two-step sequential decay pathway, the two steps are independent from each other. With the momenta  $\vec{P}_{1st}$  of the first step and  $\vec{P}_{2nd}$  of the second step, the momentum vectors  $\vec{p}_j$  with  $j = 1, 2, 3$  of the three fragments can be written as

$$\vec{p}_1 = \vec{P}_{1st}, \quad (3)$$

$$\vec{p}_2 = -\frac{m_2}{m_2 + m_3} \vec{P}_{1st} + \vec{P}_{2nd}, \quad (4)$$

$$\vec{p}_3 = -\frac{m_3}{m_2 + m_3} \vec{P}_{1st} - \vec{P}_{2nd}, \quad (5)$$

where  $j = 1$  corresponds to the fragment emitted in the first step that will not lead to other fragments and fragments  $j = 2, 3$  are emitted in the second step by the intermediate

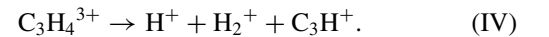
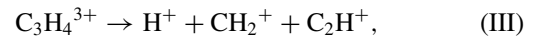
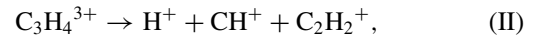
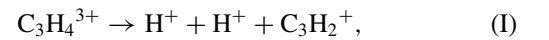
molecular ion. In the above formulas,  $\vec{P}_{1st}$  simply corresponds to the momentum of one of the fragments emitted in the first fragmentation step.  $\vec{P}_{2nd}$  corresponds to the momentum of one of the fragments emitted in the secondary fragmentation of the metastable molecular ion in the frame of its own center of mass. The momentum values of the two steps are  $|\vec{P}_{1st}| = \sqrt{2m_1(m_2 + m_3)E_1/(m_1 + m_2 + m_3)}$  and  $|\vec{P}_{2nd}| = \sqrt{2m_2m_3E_2/(m_2 + m_3)}$ , respectively, where  $m_k$  with  $k = 1, 2, 3$  denote the masses of the three fragments and  $E_1, E_2$  represent the kinetic energies released in the two steps.

### III. RESULTS AND DISCUSSION

#### A. Identification of fragmentation channels

Figure 1(a) presents the TOF spectrum of recoil ions generated from the ionization and dissociation of C<sub>3</sub>H<sub>4</sub>. Various ionic fragments are observed, including the dominant ones, i.e., parent molecular ions C<sub>3</sub>H<sub>4</sub><sup>+</sup> and C<sub>3</sub>H<sub>4</sub><sup>2+</sup>, and their daughter species. The occurrence of C<sub>3</sub>H<sub>*n*</sub><sup>2+</sup> ( $n = 2-3$ ) in the TOF spectrum indicates their rather long lifetime in the order of at least several  $\mu$ s, which further suggests a possible decay channel of parent dication or trication involving the C<sub>3</sub>H<sub>*n*</sub><sup>2+</sup> fragments as intermediate. In addition to the ions produced from the C<sub>3</sub>H<sub>4</sub> molecule, we also observed H<sub>2</sub>O<sup>+</sup>, HO<sup>+</sup>, O<sub>2</sub><sup>+</sup>, and N<sub>2</sub><sup>+</sup> peaks in the TOF spectrum, which result from the residual background molecules in the collision chamber.

In the present study, we focus on the three-body dissociation channels of C<sub>3</sub>H<sub>4</sub><sup>3+</sup>, which can be identified by the triple-ion coincidence TOF map as displayed in Fig. 1(b). In this map the sum of the TOFs of the first and second detected ions is set along the horizontal axis, while the TOF of the third detected ion is along the vertical axis. Then we identify that the four structures surrounded by red elliptic lines in Fig. 1(b) correspond to four three-body complete fragmentation channels of C<sub>3</sub>H<sub>4</sub><sup>3+</sup>. These channels are referred to as channels I, II, III, and IV as follows,



The last channel involves the formation of H<sub>2</sub> molecule and thus has a rather small cross section, which will not be analyzed in the present work. Besides the above-identified structures in the coincidence TOF map, the others are attributed to many-body fragmentation processes with the undetected fragment(s).

Channel I, C<sub>3</sub>H<sub>4</sub><sup>3+</sup>  $\rightarrow$  H<sup>+</sup> + H<sup>+</sup> + C<sub>3</sub>H<sub>2</sub><sup>+</sup>, is a recently reported three-body fragmentation channel for C<sub>3</sub>H<sub>4</sub><sup>3+</sup> trications compared to previous works [22–24]. It occurs via the breaking of two C-H bonds, while channels II and III are formed via the breakage of both C-H and C-C bonds. To largely exclude the random coincidence events, the momentum sum in each dimension of three coincidence fragments is limited to lie between  $\pm 5$  a.u. Given that the complete collection of recoil ions is affected by the extraction field,

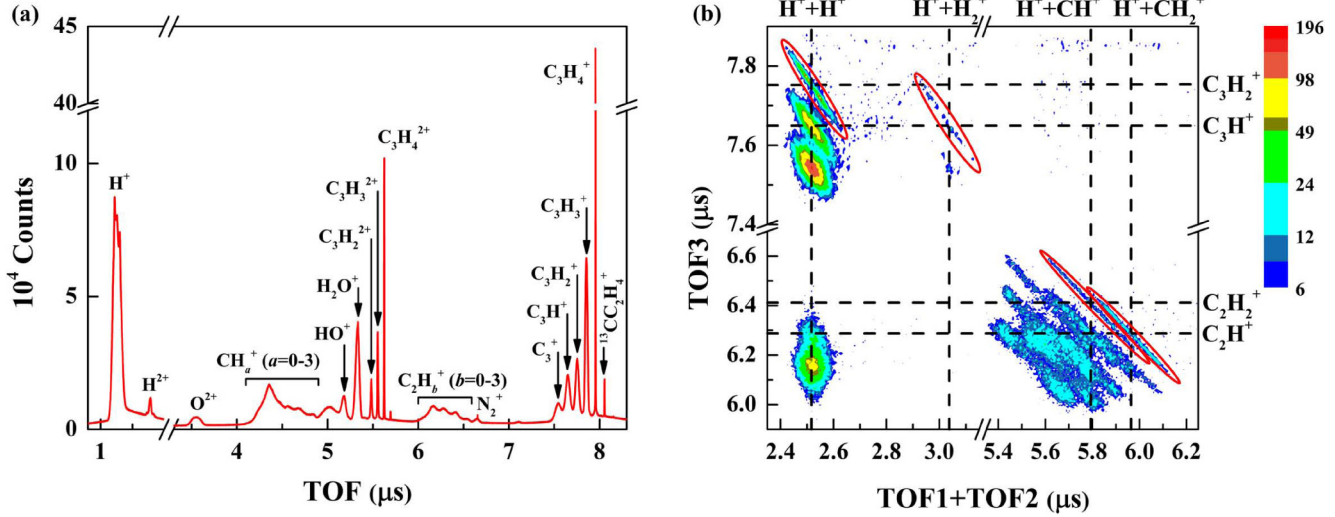


FIG. 1. (a) The TOF spectrum and (b) triple-ion coincidence TOF map of the collisions of  $C_3H_4$  with 30-keV/u  $He^{2+}$ .

during data analysis we limited the angle between the momentum of first  $H^+$  and the TOF axis to be smaller than  $30^\circ$  in each channel to avoid energetic ion losses. Under this condition and the assumption that the emission angles of the ions are isotropic, the relative fractions of these three channels can be fairly estimated. They are  $\sim 54\%$ ,  $\sim 20\%$ , and  $\sim 26\%$ , respectively, with a margin of error of about 15%, which is mainly due to the detection efficiency and statistical errors. As the three-dimensional momenta of each ionic fragment are reconstructed by the COLTRIMS technique, the kinetic energy release (KER) of a dissociation channel can be determined. The center-of-mass frame is used in reconstructing the fragment momentum in the present work. Figure 2 depicts the KER distributions of channels I–III, which range from 8 to 18 eV with peak values of 12, 12.8, and 12.8 eV, respectively. Channels II and III relate to C-C bond breaking and have a larger KER than channel I only involving C-H bond breaking.

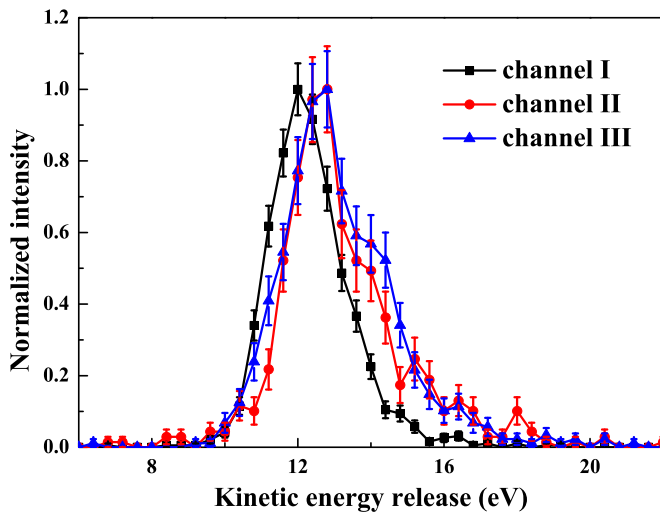


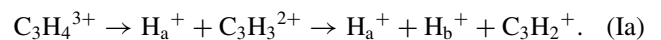
FIG. 2. KER distributions of three three-body fragmentation channels for  $C_3H_4^{3+}$ : (I)  $C_3H_4^{3+} \rightarrow H^+ + H^+ + C_3H_2^+$ , (II)  $C_3H_4^{3+} \rightarrow H^+ + CH^+ + C_2H_2^+$ , and (III)  $C_3H_4^{3+} \rightarrow H^+ + CH_2^+ + C_2H^+$ .

Such a KER difference between the C-C and C-H bond breaking channels was also found in the two-body fragmentation of  $C_3H_4^{2+}$  dications [26].

The dissociation mechanisms of channels II and III have been analyzed in an earlier work [22], whose conclusions are consistent with the present results. These channels can result from both the concerted and sequential dissociation of  $C_3H_4^{3+}$  trications. In these two channels different dissociation mechanisms correspond to different KER distributions, which leads, in addition to the main peak at 13 eV, to another KER contribution around 14 eV (see Fig. 2). However, the KER distribution of channel I exhibits a single peak, which might indicate the important role of a single dissociation mechanism in its formation. In the following section, channel I,  $C_3H_4^{3+} \rightarrow H^+ + H^+ + C_3H_2^+$ , will be analyzed in detail through the Dalitz plot and Newton diagram to identify its fragmentation mechanism. It should be noted that although the present extraction field cannot enable a complete collection of some fragments, e.g., the higher-energy protons, it does not affect the identification of fragmentation mechanisms in a three-body channel.

### B. Fragmentation channel $H^+ + H^+ + C_3H_2^+$

The Dalitz plot and Newton diagram for the channel I are shown in Figs. 3(a) and 3(b), respectively. In the Dalitz plot, three edges of the equilateral triangle represent three fragment ions, i.e., two  $H^+$  (denoted as  $H_a^+$  and  $H_b^+$  for the first and second detected protons, respectively) and  $C_3H_2^+$ . The data points are placed in the inscribed circle of the triangle and the distances of one data point from three edges represent the relative squared momenta [see formulas (1) and (2)] of three fragments. Two oblique stripe structures are distributed symmetrically on both sides of the vertical dashed line marked as regions A and B, respectively. Such a stripe structure is a typical feature of sequential dissociation [4,13,14,16,17]. Accordingly, the data points in region A correspond to the events of the following sequential channel:



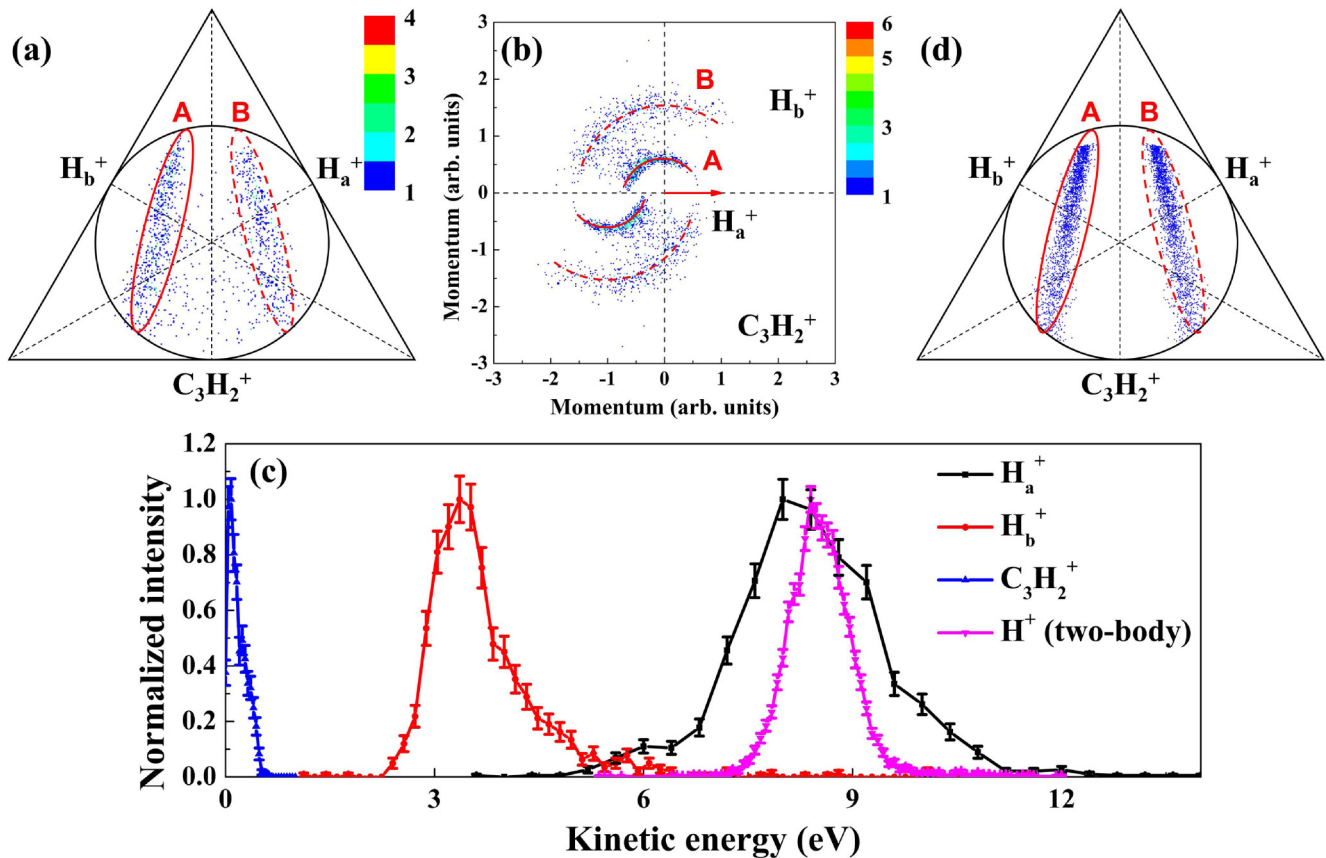


FIG. 3. (a) Dalitz plot for the  $H^+ + H^+ + C_3H_2^+$  channel. Intense areas surrounded by red ellipses of solid and dashed lines are marked as regions A and B, respectively.  $H_a^+$  represents the first detected proton, whereas  $H_b^+$  the second one. Regions A and B contain only the contribution of sequential fragmentation. (b) Newton diagram for the  $H^+ + H^+ + C_3H_2^+$  channel. The momenta of  $H_b^+$  and  $C_3H_2^+$  are normalized to the momentum of  $H_a^+$ . Red solid and dashed semicircles are plotted to guide the eye for the semicircular structures. (c) KE distributions of  $H_a^+$ ,  $H_b^+$ , and  $C_3H_2^+$  of channel I. The KE of  $H^+$  from the two-body dissociation channel  $C_3H_4^{3+} \rightarrow H^+ + C_3H_3^{2+}$  are also superimposed in the diagram. These curves are normalized to unity at the maximum. (d) Simulated Dalitz plot for the sequential dissociation process  $C_3H_4^{3+} \rightarrow H^+ + C_3H_3^{2+} \rightarrow H^+ + H^+ + C_3H_2^+$ .

In this sequential process, the  $H_a^+$  and  $H_b^+$  ions are produced in the first and second fragmentation steps, respectively. Conversely, for region B, the  $H_b^+$  ion is generated in the first fragmentation step, while the  $H_a^+$  ion arises from the second fragmentation step. Regions A and B arise from the fact that the first emitted proton can be detected before or after the second emitted proton depending on its direction of emission (towards the detector or in the opposite direction) and kinetic energy (KE). This kind of sequential deprotonation pathway has been observed in the dissociation of  $C_2H_2$  and  $C_2H_4$  trications [15–18]. In these previous studies, an intense distribution area was observed close to the edge of the Dalitz plot corresponding to the heavier fragment and indicating a concerted fragmentation process. Such a distribution close to the  $C_3H_2^+$  edge of the Dalitz plot is not observed here. This shows that a concerted fragmentation process ( $C_3H_4^{3+} \rightarrow H^+ + H^+ + C_3H_2^+$ ), where the two C-H bonds break concertedly and lead to the formation of two equivalent protons, does not occur in the present case.

In the Newton diagram, the momentum vector of the first detected proton  $H_a^+$  is set as a unit along the  $x$  axis as the red arrow shown in Fig. 3(b). The momenta of the second detected proton  $H_b^+$  and the residual  $C_3H_2^+$  are normalized

using the same normalization factor for the first detected proton  $H_a^+$  and placed respectively above and below the  $x$  axis. Two pairs of semicircular structures can be apparently seen in Fig. 3(b). The semicircular structures marked by the red solid semicircles are strong evidence of a two-step fragmentation process [4, 11, 13, 14, 16], which corresponds to region A of the Dalitz plot in Fig. 3(a). In the first step, the  $C_3H_4^{3+}$  trication breaks into the  $H_a^+$  ion and the metastable  $C_3H_3^{2+}$  ion. Then the two ions repel each other and after some time the second step happens that the metastable intermediate  $C_3H_3^{2+}$  dication breaks into the  $H_b^+$  and  $C_3H_2^+$  ions. Similarly, the other semicircular structures marked by red dashed semicircles correspond to region B of the Dalitz plot. The incomplete semicircular structures indicate that the lifetime of the intermediate  $C_3H_3^{2+}$  is shorter than its own rotation period of, e.g., ps. Since there is no reported rotational period value of  $C_3H_3^{2+}$  and the present channel does not have enough counts, we do not perform an exponential decay fitting [7] for the angle distribution between the first and second fragmentation axes to retrieve the lifetime of  $C_3H_3^{2+}$ . Again, no intense area appears in the Newton diagram and also indicates the absence of the concerted fragmentation process.

Since the structures in the Dalitz plot or Newton diagram and thus fragmentation mechanisms are clarified, the kinematics of the  $H^+ + H^+ + C_3H_2^+$  channel are explicit. The KEs of the three fragments of channel I are plotted in Fig. 3(c). As the event points in regions A and B are equivalent, we merge them for better statistics by switching  $H_a^+$  by  $H_b^+$  and  $H_b^+$  by  $H_a^+$  in region B. It can be found that the KE of the first proton is much higher than that of the second proton. Such KE distributions are consistent with the sequential fragmentation, in which the proton produced in the first step is repulsed by the doubly charged  $C_3H_3^{2+}$  and the other one by the singly charged  $C_3H_2^+$ . This leads to the higher KER of the first step  $C_3H_4^{3+} \rightarrow H_a^+ + C_3H_3^{2+}$  than that of the second step  $C_3H_3^{2+} \rightarrow H_b^+ + C_3H_2^+$ . Although the higher-energy proton was not collected completely due to the present extraction field, its KER distribution almost does not change when the angle restriction for the momenta of protons is applied to avoid the influence of energetic ion loss.

Furthermore, the KE peak value of  $\sim 8.4$  eV of the first detected proton  $H_a^+$  compares favorably with the KE of  $H^+$  in the two-body dissociation channel  $C_3H_4^{3+} \rightarrow H^+ + C_3H_3^{2+}$  as shown in Fig. 3(c). This, from another perspective, indicates the existence of a sequential dissociation mechanism. Both the two-body and three-body channels result from the same trication  $C_3H_4^{3+}$  and involve the production of  $C_3H_3^{2+}$  dication which has a different stability [5]. For the two-body one, the  $C_3H_3^{2+}$  dication is stable (or has a long lifetime) as it is detected in the present TOF spectrum. The appearance of this two-body channel is consistent with the *ab initio* calculations that  $H^+ + C_3H_3^{2+}$  is the most favorable route for the dissociation of  $C_3H_4^{3+}$  [27]. For the three-body one, there is no concerted fragmentation but a two-step process with a short lifetime. In ion-molecule collisions, the large distribution of impact parameters can lead to a broad energy-transfer distribution and involves a distribution of vibrational energy transfer [30]. As we note that the KE distribution of  $H_a^+$  is much broader than that of  $H^+$  from the two-body channel, this might show that the vibrational excitation of the  $C_3H_4^{3+}$  trication leading to three-body fragmentation is significantly larger than that leading to the two-body fragmentation process. This larger vibrational excitation could give more impetus to the hydrogen migration within the trication molecule.

To further confirm the existence of sequential fragmentation leading to channel I, we use a classical mechanical model (see Sec. II) to simulate the corresponding Dalitz plot as shown in Fig. 3(d). The released kinetic energies used in modeling are assumed to have a Gaussian distribution  $\text{Gauss}(E, \omega)$  with the mean value  $E$  and the standard deviation  $\omega$  in eV, where  $E$  corresponds to the released kinetic energy of each step. According to the experimental results,  $\text{Gauss}(8.6, 0.4)$  and  $\text{Gauss}(3.4, 0.4)$  are set to the first and second steps of pathway Ia, respectively. The angle between the first and second fragmentation axes is distributed following the experimental distribution  $\text{Gauss}(0.6\pi, 0.4\pi)$  within the range of  $\pi/6 - \pi$ . Then using formulas (1)–(5) to reconstruct the Dalitz plot, two oblique stripe structures are thus presented in

Fig. 3(d), which is in perfect agreement with the experimental Dalitz plot.

The absence of the concerted pathway ( $C_3H_4^{3+} \rightarrow H^+ + H^+ + C_3H_2^+$ ) and the presence of the sequential one ( $C_3H_4^{3+} \rightarrow H^+ + C_3H_3^{2+} \rightarrow H^+ + H^+ + C_3H_2^+$ ) in the present case indicate the two protons or corresponding hydrogen atoms in  $C_3H_4^{3+}$  trications are in different environments during dissociation, which could finally result in two different protons. One possible process responsible for the absence of the concerted pathway is the ultrafast intramolecular hydrogen migration occurring after the triple ionization of the  $C_3H_4$  molecule. The  $C_3H_4$  trication in the ground doublet electronic state has three different isomers, i.e., allene $^{3+}$ , vinylmethylene $^{3+}$ , and propyne $^{3+}$  [27]. The isomerization between them occurs by consecutive 1,2-H migrations, which exhibit significantly lower barriers. Such a hydrogen migration process has been investigated in the three-body Coulomb explosion of an allene molecule driven by the intense laser field ionization and the timescale was estimated to be  $\sim 20$  fs [24]. Once the relevant hydrogen atom(s) migrates around the C-C-C skeletal bond, the four initially equivalent H atoms in the ground state allene trication become nonequivalent, and thus the  $C_3H_4^{3+}$  trication could explode to form two different protons. Nevertheless, this supposition needs theoretical calculation, e.g., *ab initio* molecular dynamics simulation, to be clearly established.

#### IV. CONCLUSIONS

In conclusion, the three-body fragmentation dynamics of allene trications induced by the 30-keV/u  $He^{2+}$  ion impact is studied employing the COLTRIMS technique. The fragmentation pattern of the channel  $H^+ + H^+ + C_3H_2^+$  is analyzed through the Dalitz plot and Newton diagram. The results are found to be very different from previous studies of similar three-body channels because it herein only includes a sequential process, i.e.,  $C_3H_4^{3+} \rightarrow H^+ + C_3H_3^{2+} \rightarrow H^+ + H^+ + C_3H_2^+$ , and the concerted deprotonation mechanism is found to be totally absent to form this channel. Such a unique fragmentation pattern suggests that the two resultant protons or corresponding hydrogen atoms are not identical in the structure of the  $C_3H_4^{3+}$  trication. An ultrafast hydrogen migration process might occur immediately after the triple ionization of the allene molecule, which finally leads to the two different proton fragments.

#### ACKNOWLEDGMENTS

This work was supported by the National Natural Science Foundation of China under Grants No. U1832201 and No. 11674067, the National Key Research and Development Program of China under Grant No. 2017YFA0402300, and by the Shanghai Leading Academic Discipline Project (Project No. B107). Z.H. is supported by the Fundamental Research Funds for the Central Universities in China (Grant No. YJ202144).

- [1] A. Hishikawa, A. Iwamae, and K. Yamanouchi, Ultrafast Deformation of the Geometrical Structure of  $\text{CO}_2$  Induced in Intense Laser Fields, *Phys. Rev. Lett.* **83**, 1127 (1999).
- [2] I. Bocharova, R. Karimi, E. F. Penka, J.-P. Brichta, P. Lassonde, X. Fu, J.-C. Kieffer, A. D. Bandrauk, I. Litvinyuk, J. Sanderson, and F. Légaré, Charge Resonance Enhanced Ionization of  $\text{CO}_2$  Probed by Laser Coulomb Explosion Imaging, *Phys. Rev. Lett.* **107**, 063201 (2011).
- [3] C. Wu, C. Wu, D. Song, H. Su, Y. Yang, Z. Wu, X. Liu, H. Liu, M. Li, Y. Deng, Y. Liu, L.-Y. Peng, H. Jiang, and Q. Gong, Nonsequential and Sequential Fragmentation of  $\text{CO}_2^{3+}$  in Intense Laser Fields, *Phys. Rev. Lett.* **110**, 103601 (2013).
- [4] N. Neumann, D. Hant, L. P. H. Schmidt, J. Titze, T. Jahnke, A. Czasch, M. S. Schöffler, K. Kreidi, O. Jagutzki, H. Schmidt-Böcking, and R. Dörner, Fragmentation Dynamics of  $\text{CO}_2^{3+}$  Investigated by Multiple Electron Capture in Collisions with Slow Highly Charged Ions, *Phys. Rev. Lett.* **104**, 103201 (2010).
- [5] L. Wei, B. Ren, Y. Zhang, J. Wang, B. Wang, J. Han, W. Yu, Y. Zou, L. Chen, and B. Wei, Delayed fragmentation of ethylene and allene induced by electron impact, *Phys. Rev. A* **103**, 012810 (2021).
- [6] X. Ding, M. Haertelt, S. Schlauderer, M. S. Schuurman, A. Y. Naumov, D. M. Villeneuve, A. R. W. McKellar, P. B. Corkum, and A. Staudte, Ultrafast Dissociation of Metastable  $\text{CO}^{2+}$  in a Dimer, *Phys. Rev. Lett.* **118**, 153001 (2017).
- [7] J. Rajput, H. Kumar, P. Bhatt, and C. P. Safvan, A new technique for measurement of subrotational lifetime of molecular ions, *Sci. Rep.* **10**, 20301 (2020).
- [8] A. Méry, X. Flécharde, S. Guillous, V. Kumar, M. Lalande, J. Rangama, W. Wolff, and A. Cassimi, Investigation of the carbon monoxide dication lifetime using  $(\text{CO})_2$  dimer fragmentation, *Phys. Rev. A* **104**, 042813 (2021).
- [9] T. Endo, S. P. Neville, V. Wanie, S. Beaulieu, C. Qu, J. Deschamps, P. Lassonde, B. E. Schmidt, H. Fujise, M. Fushitani, A. Hishikawa, P. L. Houston, J. M. Bowman, M. S. Schuurman, F. Légaré, and H. Ibrahim, Capturing roaming molecular fragments in real time, *Science* **370**, 1072 (2020).
- [10] P. Bhatt, R. Singh, N. Yadav, and R. Shanker, Momentum spectroscopy of fragment ions of a multiply charged  $\text{N}_2\text{O}$  molecule under impact of 10-keV electrons, *Phys. Rev. A* **86**, 052708 (2012).
- [11] E. Wang, M. Gong, Z. Shen, X. Shan, X. Ren, A. Dorn, and X. Chen, Fragmentation dynamics of  $\text{CS}_2$  in collisions with 1.0 keV electrons, *J. Chem. Phys.* **149**, 204301 (2018).
- [12] M. R. Jana, P. N. Ghosh, B. Bapat, R. K. Kushawaha, K. Saha, I. A. Prajapati, and C. P. Safvan, Ion-induced triple fragmentation of  $\text{CO}_2^{3+}$  into  $\text{C}^+ + \text{O}^+ + \text{O}^+$ , *Phys. Rev. A* **84**, 062715 (2011).
- [13] A. Khan, L. C. Tribedi, and D. Misra, Three-body fragmentation of multiply charged nitrous oxide induced by  $\text{Ar}^{8+}$ - and  $\text{Xe}^{15+}$ -ion impact, *Phys. Rev. A* **96**, 012703 (2017).
- [14] B. Wang, J. Han, X. Zhu, L. Wei, B. Ren, Y. Zhang, W. Yu, S. Yan, X. Ma, Y. Zou, L. Chen, and B. Wei, Dissociative ionization of  $\text{OCS}$  induced by highly charged ion impact, *Phys. Rev. A* **103**, 042810 (2021).
- [15] T. Jiang, B. Wang, Y. Zhang, L. Wei, S. Chen, W. Yu, Y. Zou, L. Chen, and B. Wei, Three-fragment dissociation of  $\text{C}_2\text{H}_2^{2+}$  and  $\text{C}_2\text{H}_2^{3+}$  produced by slow- $\text{Ar}^{8+}$ -ion impact, *Phys. Rev. A* **100**, 022705 (2019).
- [16] S. Xu, X. L. Zhu, W. T. Feng, D. L. Guo, Q. Zhao, S. Yan, P. Zhang, D. M. Zhao, Y. Gao, S. F. Zhang, J. Yang, and X. Ma, Dynamics of  $\text{C}_2\text{H}_2^{3+} \rightarrow \text{H}^+ + \text{H}^+ + \text{C}_2^+$  investigated by 50-keV/u  $\text{Ne}^{8+}$  impact, *Phys. Rev. A* **97**, 062701 (2018).
- [17] B. Ren, Z. Xia, Y. Zhang, L. Wei, W. Yu, J. Han, B. Wang, Y. Zou, L. Chen, and B. Wei, Three-body fragmentation mechanism of  $\text{C}_2\text{H}_4^{3+}$  produced by 18-keV/u  $\text{Ne}^{8+}$  impact, *Phys. Rev. A* **104**, 022811 (2021).
- [18] X. Xie, E. Lötstedt, S. Roither, M. Schöffler, D. Kartashov, K. Midorikawa, A. Baltuška, K. Yamanouchi, and M. Kitzler, Duration of an intense laser pulse can determine the breakage of multiple chemical bonds, *Sci. Rep.* **5**, 12877 (2015).
- [19] J. Zhou, Y. Li, Y. Wang, S. Jia, X. Xue, T. Yang, Z. Zhang, A. Dorn, and X. Ren, Ultrafast ring-opening fragmentation dynamics of  $\text{C}_6\text{H}_6^{3+}$  induced by electron-impact ionization, *Phys. Rev. A* **104**, 032807 (2021).
- [20] S. W. J. Scully, V. Senthil, J. A. Wyer, M. B. Shah, E. C. Montenegro, M. Kimura, and H. Tawara, Direct evidence of a strong isomer effect in electron-impact double ionization of  $\text{C}_3\text{H}_4$ , *Phys. Rev. A* **72**, 030701(R) (2005).
- [21] T. Kusakabe, S. Satoh, H. Tawara, and M. Kimura, Observation of the Isomer Effect on Charge Transfer from  $\text{C}_3\text{H}_4$  Molecules (Allene and Propyne) at keV Energies, *Phys. Rev. Lett.* **87**, 243201 (2001).
- [22] C. Ma, S. Xu, D. Zhao, D. Guo, S. Yan, W. Feng, X. Zhu, and X. Ma, Three-body fragmentation dynamics of  $\text{CH}_2\text{CCH}_2^{3+}$  investigated by 50-keV/u  $\text{Ne}^{8+}$  impact, *Phys. Rev. A* **101**, 052701 (2020).
- [23] H. Xu, T. Okino, and K. Yamanouchi, Tracing ultrafast hydrogen migration in allene in intense laser fields by triple-ion coincidence momentum imaging, *J. Chem. Phys.* **131**, 151102 (2009).
- [24] H. Xu, T. Okino, and K. Yamanouchi, Ultrafast delocalization of hydrogen atoms in allene in intense laser fields, *Appl. Phys. A* **104**, 941 (2011).
- [25] H. Xu, T. Okino, and K. Yamanouchi, Ultrafast hydrogen migration in allene in intense laser fields: Evidence of two-body Coulomb explosion, *Chem. Phys. Lett.* **469**, 255 (2009).
- [26] Y. Li, S. Xu, D. Guo, S. Jia, X. Jiang, X. Zhu, and X. Ma, Two-body dissociation of  $\text{C}_3\text{H}_4$  isomers investigated by 50 keV/u  $\text{Ne}^{8+}$  impact, *J. Chem. Phys.* **150**, 144311 (2019).
- [27] A. M. Mebel and A. D. Bandrauk, Theoretical study of unimolecular decomposition of allene cations, *J. Chem. Phys.* **129**, 224311 (2008).
- [28] J. Ullrich, R. Moshhammer, A. Dorn, R. Dörner, L. P. H. Schmidt, and H. Schmidt-Böcking, Recoil-ion and electron momentum spectroscopy: Reaction-microscopes, *Rep. Prog. Phys.* **66**, 1463 (2003).
- [29] Y. Zhang, T. Jiang, L. Wei, D. Luo, X. Wang, W. Yu, R. Hutton, Y. Zou, and B. Wei, Three-body fragmentation of methane dications produced by slow  $\text{Ar}^{8+}$ -ion impact, *Phys. Rev. A* **97**, 022703 (2018).
- [30] S. Maclot, R. Delaunay, D. G. Piekarski, A. Domaracka, B. A. Huber, L. Adoui, F. Martín, M. Alcamí, L. Avaldi, P. Bolognesi, S. Díaz-Tendero, and P. Rousseau, Determination of Energy-Transfer Distributions in Ionizing Ion-Molecule Collisions, *Phys. Rev. Lett.* **117**, 073201 (2016).